Single-Delta Bridge-Cell Converter With Single Single-Phase Medium-Frequency Transformer Capable of Active Power Control

Makoto Hagiwara, *Senior Member, IEEE*, Yoshihito Chuman, and Yuki Kudo

***Abstract*—A modular multilevel cascade converter based on single-delta bridge cells, hereinafter referred to as the single-delta bridge-cell (SDBC) converter, is a prospective power converter for a static synchronous compensator intended for voltage regulation and stability improvement of electric power systems. However, the SDBC converter cannot exchange nonzero active power with the three-phase ac mains unless energy storage elements such as batteries are connected to the dc side of each bridge cell. This article presents a dc/1ϕ/3ϕ power converter that combines the SDBC converter with a single-phase converter via a single-phase medium-frequency transformer with an operating frequency of 150 Hz. It can control the active power of 37% of the rated reactive power between the dc source and three-phase ac mains, thus enhancing voltage regulation and stability improvement. The operating principles and control method are first discussed, followed by a description of experiments using a downscaled 110-V, 5-kVA model.**

***Index Terms*—Modular multilevel cascade converters, single-delta bridge-cell (SDBC) converter, static synchronous compensator (STATCOM).**

I. Introduction

STATIC synchronous compensators (STATCOMs) with a power rating greater than several tens of MVA have been implemented for the voltage regulation and stability improvement of electric power systems [1]–[3]. A modular multilevel cascade converter based on single-delta bridge cells (SDBC) [4], [5], hereinafter referred to as the SDBC converter according to the classification shown in [6], is a prospective transformerless converter for STATCOMs owing to its redundancy, fast controllability, and low harmonic voltages. Fig. 1 shows the circuit configuration of the conventional SDBC converter for STATCOMs, where three clusters are connected via a common coupled inductor. Numerous studies have investigated the SDBC converter for STATCOMs with a focus on the control and modulation methods, low-voltage ride-through capability, negative-sequence reactive power compensation, and comparison with other topologies [7]–[19]. Recently, a STATCOM based on the SDBC converter for electric power systems has been implemented in the United States [15].

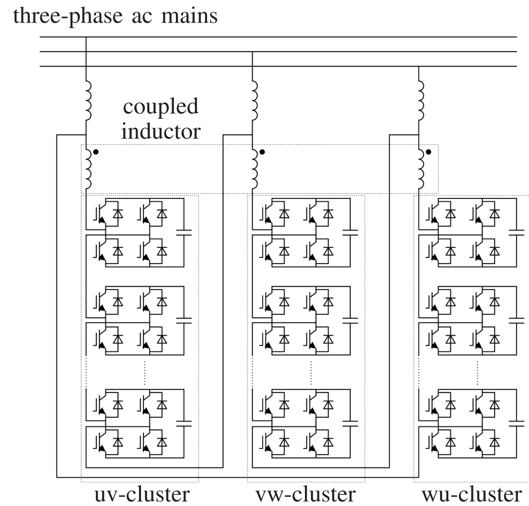

Fig. 1. Circuit configuration of the conventional SDBC converter for a STATCOM.

In general, the SDBC converter cannot exchange nonzero active power with the three-phase ac mains, and additional components (e.g., dc sources, circuits, transformers, and so on) must be used for active power control, which may result in significant increases in terms of mass, volume, and cost. This problem is common to other modular multilevel cascade converter topologies as well. One of the methods to achieve active power control is to connect energy storage elements such as photovoltaic (PV) arrays or batteries to the dc side of each bridge cell. Sochor and Akagi [20], [21] designed and developed a solar power generation system based on the SDBC converter, where multiple PV arrays along with an isolated dc–dc converter are connected to the dc capacitor of each bridge cell. As a result, nonzero active power can be exchanged between PV arrays and the three-phase ac mains. However, the control system of the SDBC converter becomes complex, because it has to take into account the imbalance of power generation from all the PV arrays. Furthermore, many high-frequency transformers are

Manuscript received November 10, 2020; revised February 1, 2021 and March 22, 2021; accepted April 22, 2021. Date of publication April 27, 2021; date of current version July 30, 2021. This work was supported in part by the Council for Science, Technology, and Innovation, in part by the Cross-Ministerial Strategic Innovation Promotion Program, and in part by the Next-Generation Power Electronics, and funded by the New Energy and Industrial Technology Development Organization. Recommended for publication by Associate Editor P. Mattavelli. *(Corresponding author: Makoto Hagiwara.)*

The authors are with the Department of Electrical, and Electronics Engineering, Tokyo Institute of Technology, Tokyo 152-8552, Japan (e-mail: hagiwara@ee.e.titech.ac.jp; chuman.y.aa@m.titech.ac.jp; yuki5.kudo@toshiba.co.jp).

Color versions of one or more figures in this article are available at https://doi.org/10.1109/TPEL.2021.3076163.

Digital Object Identifier 10.1109/TPEL.2021.3076163

required for galvanic isolation, which may result in high cost and low reliability. A similar problem occurs when PV arrays are replaced with batteries.

The author of this article has proposed a dc/1ϕ/3ϕ power converter that combines the SDBC converter with a single-phase converter via a single single-phase medium-frequency transformer in [22]–[24]. The converter is characterized by a connection between the three clusters of the SDBC converter through the secondary windings of the transformer, which are divided into three equal parts and each cluster is connected to the corresponding part. The primary windings are connected to the single-phase converter via an ac inductor, where concentrated energy storage elements such as batteries are connected to the dc side. Consequently, dc/1ϕ/3ϕ power conversion and galvanic isolation can be achieved simultaneously using a single transformer and a single dc power source. Furthermore, an existing SDBC converter can be applied without changing the voltage and current ratings, where the control method is basically the same as that of the SDBC converter for STATCOMs except for some modifications that will be described in Section IV. The operating principles and control method of the converter have not been fully discussed in [22]–[24], and no experimental verification has been reported. The comparison of the dc/1ϕ/3ϕ converter and that presented in [20] and [21] in terms of mass, volume, and cost is beyond the scope of this article and left for future work.

It is known that a modular multilevel cascade converter based on double-star bridge cells [25], which is referred to as the DSBC converter according to the classification shown in [6], can also achieve dc/1ϕ/3ϕ power conversion by connecting a single single-phase medium-frequency transformer to the common dc link, and applications to electric railways, quick chargers for electric vehicles, and wind power generation systems have been reported [26]–[31]. Meanwhile, the number of power devices required for the DSBC converter is $2/\sqrt{3}$ times that required for the SDBC converter, assuming that power devices with the same voltage ratings are used [6].

The aim of this article is to demonstrate the validity and effectiveness of the dc/1ϕ/3ϕ power converter that combines the SDBC converter with a single-phase converter via a medium-frequency transformer. A downscaled experimental model is designed and built to verify the operating principles and control method of the converter, where experimental waveforms with different modes of operation are presented. It is shown that an active power of 37% of the rated reactive power can be controlled without increasing the voltage and current ratings of the SDBC converter by setting the transformer frequency to 150 Hz, which is three times the line frequency of 50 Hz. This means that if the power rating of the converter is 100 MVA, the maximum exchangeable active power is 37 MW.

It should be noted that the main function of the converter is reactive power control similar to the conventional SDBC converter, and active power control is an additional function. In other words, the converter is not intended to be applied for applications where only active power control is required, such as electric railways, quick chargers for electric vehicles, and wind power generation systems described above. Examples of suitable applications for the converter will be described in Section II-D in detail.

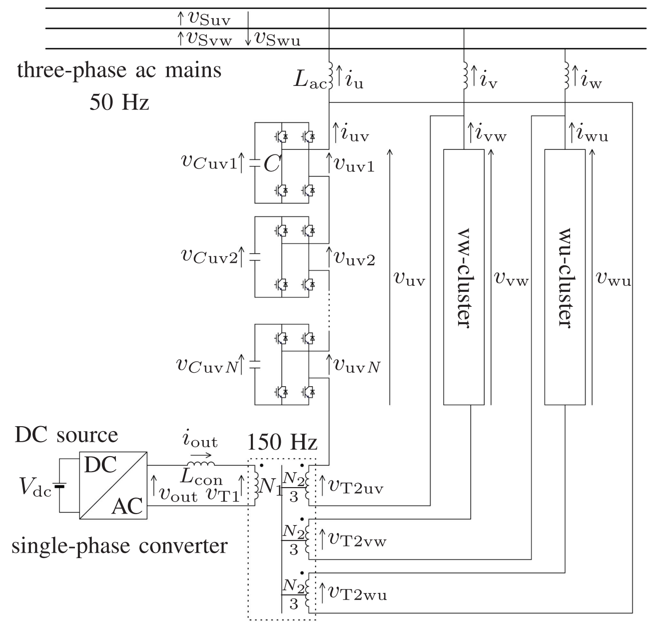

Fig. 2. Circuit configuration of a dc/1ϕ/3ϕ power converter combining the SDBC converter with a single-phase converter via a single-phase medium-frequency transformer.

The rest of this article is organized as follows. Section II explains the circuit configuration and characteristics of the proposed converter. Sections III and IV present the operating principles and control method of the proposed converter. Section V describes the experimental verification using a downscaled 110-V, 5-kVA model. Finally, Section VI concludes this article.

II. Circuit Configuration and Characteristics

A. Circuit Configuration

Fig. 2 shows the circuit configuration of a dc/1ϕ/3ϕ power converter, which comprises single-phase converter(s), a single-phase medium-frequency transformer, and the SDBC converter. Each cluster of the SDBC converter comprises cascaded bridge cells (i.e., single-phase full-bridge PWM converters), where the bridge-cell count per cluster is N. The three clusters of the conventional SDBC converter are delta-connected via a single coupled inductor, as shown in Fig. 1. The circuit shown in Fig. 2 connects the three clusters via the secondary windings of the transformer, where the windings are divided into three equal parts and each cluster is connected to the corresponding part. The operating frequency of the transformer is set to 150 Hz, which is three times the line frequency of 50 Hz, and the reason for choosing this frequency will be described in Section III. The primary windings of the transformer are connected to the single-phase converter via an ac inductor L_{con}, while each cluster is connected to the three-phase ac mains via ac-link inductors L_{ac}. It should be noted that the three noncoupled ac-link inductors can be placed within the delta connection, whereas the circulating current i_Z defined by (4) later also flows in L_{ac}, and a voltage drop originating from i_Z occurs in L_{ac}.

This makes the decoupled control of the supply currents and the circulating current difficult. This problem can be solved using a three-phase inductor with a three-legged core as the inductor presents inductance only to the positive/negative sequence component and presents zero inductance to the zero-sequence component. The SDBC converter can increase the voltage rating easily by increasing the bridge-cell count N.

v_{Suv}, v_{Svw}, and v_{Swu} are the supply line-to-line voltages represented by

$$\begin{aligned} v_{\mathrm{Suv}} &= \sqrt{2}V_{\mathrm{S}}\sin\left(\omega t + \frac{\pi}{6}\right)\\ v_{\mathrm{Svw}} &= \sqrt{2}V_{\mathrm{S}}\sin\left(\omega t - \frac{\pi}{2}\right)\\ v_{\mathrm{Swu}} &= \sqrt{2}V_{\mathrm{S}}\sin\left(\omega t - \frac{7\pi}{6}\right) \end{aligned} \tag{1}$$

where V_{S} is the root-mean-square (rms) value. v_{Coi} ($o \in \{\mathrm{uv}, \mathrm{vw}, \mathrm{wu}\}, i \in \{1\ldots N\}$) is the dc-capacitor voltage, v_{oi} is the ac voltage of each bridge cell, and v_o is the cluster voltage. The following relationship holds between v_{oi} and v_o:

$$v_o = \sum_{i=1}^{N} v_{oi}. \tag{2}$$

i_{uv}, i_{vw}, and i_{wu} are the cluster currents, and i_{u}, i_{v}, and i_{w} are the supply currents, where the following relationships hold:

$$\begin{aligned} i_{\mathrm{u}} &= i_{\mathrm{uv}} - i_{\mathrm{wu}}\\ i_{\mathrm{v}} &= i_{\mathrm{vw}} - i_{\mathrm{uv}}\\ i_{\mathrm{w}} &= i_{\mathrm{wu}} - i_{\mathrm{vw}}. \end{aligned} \tag{3}$$

Let the circulating current flowing in the delta-connected windings be i_Z. According to [9], it is given by

$$i_Z = \frac{1}{3}(i_{\mathrm{uv}} + i_{\mathrm{vw}} + i_{\mathrm{wu}}). \tag{4}$$

The number of turns of the primary windings is N_1 and that of the secondary windings is N_2. Because the secondary windings are divided into three equal parts, each part has $N_2/3$ number of turns. v_{T1} is the primary voltage, and v_{T2uv}, v_{T2vw}, and v_{T2wu} are the secondary voltages. i_{out} is the primary current, v_{out} is the ac voltage of the single-phase converter, and V_{dc} is the dc source voltage.

B. Comparison Between SDBC and DSCC Converters

This section compares the SDBC converter and a modular multilevel cascade converter based on double-star chopper cells, which is referred to as a DSCC converter according to the classification shown in [6]. In general, the DSCC converter itself cannot perform dc/1ϕ/3ϕ power conversion, whereas it can perform dc/1ϕ/3ϕ power conversion if an additional high voltage conversion ratio dc–dc converter is applied to the common dc link of the DSCC converter. An input-series-output-parallel modular dc–dc converter presented, e.g., in [32], is one method to achieve such voltage conversion where multiple medium- or high-frequency transformers are used for galvanic isolation. Hence, it may suffer from high cost and low reliability because of many transformers required. Fig. 2 circuit can achieve dc/1ϕ/3ϕ power conversion using a "single" single-phase medium-frequency transformer, which is more suitable than the DSCC converter for high-power applications where high reliability is of extreme importance. Hence, the DSCC converter is eliminated from selection. The detail comparison between both converters in terms of mass, volume, and cost under dc/1ϕ/3ϕ power conversion is beyond the scope of this article and left for the future work.

C. Comparison Between SDBC and DSBC Converters

The biggest difference between the SDBC and DSBC converters is that the former requires no additional cells to achieve active power control, as explained later, whereas the latter must use additional cells to achieve active power control. Consequently, the number of power devices required for the SDBC converter is $\sqrt{3}/2$ times or less compared to that required for the DSBC converter. This interesting difference occurs because the positive-side and negative-side arms of the DSBC converter should produce the fundamental frequency components with the same amplitude but with a phase difference of 180°. Meanwhile, each cell in one cluster of the SDBC converter produces the fundamental frequency component with the same amplitude and the same phase; hence, active power control is achievable without the need of additional cells.

D. Characteristics of Fig. 2

The circuit shown in Fig. 2 can achieve active power control in addition to reactive power control, and this attractive feature can be used for the transient stability improvement of electric power systems. In other words, the circuit operates like the conventional synchronous phase modifier (i.e., the synchronous generator), where it charges or discharges active power by adjusting the rotating speed, and this feature cannot be achieved by the circuit shown in Fig. 1, in which only reactive power is adjustable. Furthermore, Fig. 2 circuit can achieve better performance than Fig. 1 circuit in terms of voltage regulation because it can compensate for the resistance and inductance components of transmission voltage simultaneously, whereas Fig. 1 circuit can inherently compensate for only the inductance component.

In general, a STATCOM intended for the transient stability improvement of electric power systems works only under a system disturbance such as a ground fault condition. In other words, it does not contribute to the power systems under normal conditions. Fig. 2 circuit can work as a battery energy storage system or a solar power generation system under normal conditions owing to the capability of active power control, which results in better utilization of electrical facilities. Another attractive feature of Fig. 2 circuit is that it is relatively easy to apply an existing SDBC converter to it because the voltage and current ratings of the converter do not need to be changed, and the same control system of the SDBC converter can be applied to Fig. 2 circuit except for some modifications that will be described in Section IV. Consequently, significant cost reduction could be achieved compared with the case of newly installing Fig. 2 circuit.

It is noteworthy that the main function of typical battery energy storage systems or solar power generation systems is active power control, and reactive power control for voltage regulation is an additional function. By contrast, the main function of Fig. 2 circuit is reactive power control similar to the conventional SDBC converter, and active power control is an additional function. Hence, the main and additional functions are opposite for Fig. 2 circuit in comparison with battery energy storage systems or solar power generation systems.

III. Operating Principles

A. Transformer Frequency and Voltage

The following assumptions have been introduced as follows.

1) The supply voltages are three-phase balanced voltages with no harmonic components.
2) The leakage inductance and resistance of the transformer are zero.
3) The harmonic voltages produced by each cluster are zero.
4) The ON-state voltages of the power devices, the wiring resistance, and the wiring inductance are zero.

The first assumption is introduced to simplify circuit analysis, and it is reasonable under normal conditions. The second assumption is introduced because these parameters have little effect on circuit operation. The third assumption is valid when the phase-shifted PWM is applied to each cell, and the validity of this assumption will be confirmed experimentally later. The fourth assumption is valid because the on-state voltages are negligible compared with the ac mains voltage, which is as high as several tens of kilovolts in an actual system.

The cluster voltages v_{uv}, v_{vw}, and v_{wu} in Fig. 2 have 50-Hz positive-sequence components with the same amplitude while a phase difference of 120° exists relative to each other, and the common medium-frequency zero-sequence component with the same amplitude and phase. The zero-sequence component that is applied to the secondary windings of the transformer plays an important role in active power exchange between the single-phase converter and the SDBC converter. Let the supply angular frequency be ω, and the transformer angular frequency and the initial phase be ω_{Trans} and ϕ, respectively, where the relationship $\omega < \omega_{\mathrm{Trans}}$ holds. The cluster voltages are represented by

$$\begin{aligned} v_{\mathrm{uv}} &= \sqrt{2}V_{\mathrm{S}}\sin\left(\omega t + \frac{\pi}{6}\right) - \sqrt{2}aV_{\mathrm{S}}\sin(\omega_{\mathrm{Trans}}t + \phi) \\ v_{\mathrm{vw}} &= \sqrt{2}V_{\mathrm{S}}\sin\left(\omega t - \frac{\pi}{2}\right) - \sqrt{2}aV_{\mathrm{S}}\sin(\omega_{\mathrm{Trans}}t + \phi) \\ v_{\mathrm{wu}} &= \sqrt{2}V_{\mathrm{S}}\sin\left(\omega t - \frac{7\pi}{6}\right) - \sqrt{2}aV_{\mathrm{S}}\sin(\omega_{\mathrm{Trans}}t + \phi) \end{aligned} \tag{5}$$

where a is the ratio of the medium-frequency component to the 50-Hz component. It is noteworthy that the actual v_{uv}, v_{vw}, and v_{wu} contain additional voltage components for current and dc-capacitor voltage control, as will be described in Section IV. They are set to zero in (5) because they have no effect on the transformer operation.

In (5), a can be set to a desired value within hardware limitations, and ϕ can be set to an arbitrary value. ω_{Trans} should be set to an integer multiple of 3ω for the symmetrical operation of each cluster. Furthermore, the converter and transformer loss in the Fig. 2 circuit should be minimized considering that it is expected to be applied to a high-power converter, where efficiency improvement is the top priority. In other words, ω_{Trans} should be minimized to minimize the transformer iron loss. Hence, it is set to

$$\omega_{\mathrm{Trans}} = 3\omega \tag{6}$$

which is three times the supply angular frequency.

From Kirchhoff's voltage law, the following voltage relationship holds in the delta-connected windings:

$$v_{\mathrm{uv}} + v_{\mathrm{vw}} + v_{\mathrm{wu}} = -(v_{\mathrm{T2uv}} + v_{\mathrm{T2vw}} + v_{\mathrm{T2wu}}) = -v_{\mathrm{T2}} \tag{7}$$

where v_{T2} is the sum of the secondary voltages. Equations (5) and (7) indicate that only the zero-sequence voltage included in each cluster voltage appears in v_{T2}. The relationship $v_{\mathrm{T2uv}} = v_{\mathrm{T2vw}} = v_{\mathrm{T2wu}}$ holds because each cluster produces the same zero-sequence voltage in terms of the amplitude and phase as shown in (5). Consequently, the following relationship exists in (7):

$$v_{\mathrm{T2uv}} = v_{\mathrm{T2vw}} = v_{\mathrm{T2wu}} = \frac{v_{\mathrm{T2}}}{3}. \tag{8}$$

From (5), (6), and (8), the following voltage is superimposed on each part of the secondary windings:

$$v_{\mathrm{T2uv}} = v_{\mathrm{T2vw}} = v_{\mathrm{T2wu}} = \sqrt{2}aV_{\mathrm{S}}\sin(3\omega t + \phi). \tag{9}$$

As mentioned previously, an existing SDBC converter working as a STATCOM may be applied to Fig. 2 circuit, where the voltage and current ratings cannot be changed easily. For this reason, the voltage and current ratings of the SDBC converter should be the same regardless of STATCOM operation or dc/1ϕ/3ϕ converter operation. Hence, the maximum cluster voltage should be less than or equal to $\sqrt{2}V_{\mathrm{S}}$ in (5) even when the zero-sequence component is superimposed. On the other hand, a should be as high as possible to exchange the active power with the minimum current. From (5), (6), and the abovementioned consideration regarding the cluster voltage, the maximum value of a is obtained, with the help of numerical analysis, when

$$\phi = -\frac{\pi}{2} \tag{10}$$

as

$$a = \frac{2}{5}. \tag{11}$$

Finally, a voltage with a frequency of 150 Hz, an initial phase of $-\pi/2$, and an rms value of $0.4V_{\mathrm{S}}$ is applied to each part of the secondary windings. It should be noted that ϕ and a can be set to other values as long as the cluster voltage is less than or equal to $\sqrt{2}V_{\mathrm{S}}$ in (5). However, the maximum value of a is given by (11) and is obtained when ϕ is given by (10).

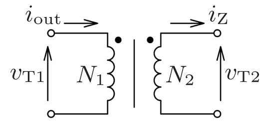

Fig. 3. Equivalent circuit of a single-phase medium-frequency transformer shown in Fig. 2.

B. Transformer Equivalent Circuit

The cluster currents (i.e., the secondary currents of the transformer) can be divided into components originating from the supply currents and the one circulating in the delta-connected windings, according to [9]. They can be described as follows:

$$\begin{aligned} i_{\mathrm{uv}} &= \frac{i_{\mathrm{u}} - i_{\mathrm{v}}}{3} + i_Z \\ i_{\mathrm{vw}} &= \frac{i_{\mathrm{v}} - i_{\mathrm{w}}}{3} + i_Z \\ i_{\mathrm{wu}} &= \frac{i_{\mathrm{w}} - i_{\mathrm{u}}}{3} + i_Z. \end{aligned} \tag{12}$$

It should be noted that (12) holds regardless of the four assumptions described at the beginning of Section III. Because the sum of the first terms on the right-hand side in (12) is zero, only the circulating current i_Z contributes to the production of electromagnetic force in the transformer. Furthermore, the transformer shown in Fig. 2 can be changed to the circuit shown in Fig. 3 equivalently, because (8) holds, and the common circulating current flows in each part of the secondary windings.

In Fig. 3, v_{T2} comprises the 50-Hz fundamental-frequency component represented by $v_{\mathrm{T2\_50}}$ and the 150-Hz medium-frequency component represented by $v_{\mathrm{T2\_150}}$, where the relationship $v_{\mathrm{T2}} = v_{\mathrm{T2\_50}} + v_{\mathrm{T2\_150}}$ holds. The power balance of each cluster can be achieved by adjusting $v_{\mathrm{T2\_50}}$ appropriately [9], while $v_{\mathrm{T2\_150}}$ is used for active power exchange between the single-phase converter and the SDBC converter. Similarly, v_{T1} comprises the 50-Hz and 150-Hz components because the relationship $v_{\mathrm{T1}} = (N_1/N_2)v_{\mathrm{T2}}$ holds in Fig. 3. The 50-Hz component should be eliminated from the primary circuit because it does not contribute to active power exchange, and this can be eliminated such that the single-phase converter produces the same 50-Hz component in terms of the amplitude and phase included in v_{T1}, as will be shown later in Fig. 8. Consequently, no 50-Hz component occurs in i_{out}.

Meanwhile, i_Z comprises the 50-Hz fundamental-frequency component represented by i_{Z_50} and the 150-Hz medium-frequency component represented by i_{Z_150}. The following relationship holds for the 50-Hz component:

$$v_{\mathrm{T2\_50}} = L_M \frac{d(i_{Z\_50})}{dt}. \tag{13}$$

In (13), L_M is the magnetizing inductance of the transformer that is represented by [9]

$$L_M = \frac{N_2^2}{R_M} \tag{14}$$

where R_M is the magnetic resistance. It should be noted that i_{Z_50} does not contribute to active power exchange, whereas it contributes to the power balance of the clusters [9].

The 150-Hz component represented by i_{Z_150} comprises the magnetizing current represented by i_{Zm_150}, and the current contributing to the active power exchange is represented by i_{Za_150}, where the relationship $i_{Z\_150} = i_{Zm\_150} + i_{Za\_150}$ holds. The following relationship holds for i_{Zm_150}

$$v_{\mathrm{T2\_150}} = L_M \frac{d(i_{Zm\_150})}{dt} \tag{15}$$

and the following relationship holds for i_{Za_150}:

$$i_{Za\_150} = \frac{N_1}{N_2} i_{\mathrm{out}}. \tag{16}$$

Equations (15) and (16) indicate that the active power exchange is irrelevant to L_M. Instead, it is related to L_{con} and the leakage inductance of the transformer as in the conventional grid-connected converter.

C. Power Rating of the Fig. 2 Circuit

The rated cluster current of the Fig. 2 circuit should be less than or equal to that of the Fig. 1 circuit, considering that an existing SDBC converter may be applied to the former circuit. Let the rms value of the supply currents i_{u}, i_{v}, and i_{w} be I. The cluster current is $I/\sqrt{3}$ when the positive-sequence reactive power is controlled, and $2I/\sqrt{3}$ when the negative-sequence reactive power is controlled, according to [9]. In general, a STATCOM for utility applications is not required to control the negative-sequence reactive power; hence, the rated cluster rms current is set to $I/\sqrt{3}$.

The following assumes that the positive active power flows to the three-phase ac mains from the dc source in Fig. 2, and no reactive power exists in the ac mains. Consequently, the 50-Hz components included in v_{uv} and i_{uv} are in phase. Let ω_{Trans}, ϕ, and a be given by (6), (10), and (11), respectively. v_{uv} in (5) can be changed to

$$v_{\mathrm{uv}} = \sqrt{2}V_{\mathrm{S}} \sin\left(\omega t + \frac{\pi}{6}\right) - \sqrt{2}\frac{2V_{\mathrm{S}}}{5} \sin\left(3\omega t - \frac{\pi}{2}\right). \tag{17}$$

When the 50-Hz components included in v_{uv} and i_{uv} are in phase and those included in v_{T2} $(= 3v_{\mathrm{T2uv}})$ and i_{out} are in phase, i_{uv} is given by

$$i_{\mathrm{uv}} = \sqrt{2}I_{50a} \sin\left(\omega t + \frac{\pi}{6}\right) + \sqrt{2}I_{150a} \sin\left(3\omega t - \frac{\pi}{2}\right) \tag{18}$$

where I_{50a} and I_{150a} are the rms values of the 50 and 150-Hz components, respectively.

Meanwhile, the following relationship should hold in (17) and (18) for regulating each dc-capacitor voltage:

$$\int_0^{2\pi/\omega} (v_{\mathrm{uv}} \times i_{\mathrm{uv}}) dt = 0 \tag{19}$$

where $2\pi/\omega$ is the period of the three-phase ac mains $(= 20$ ms). Substituting (17) and (18) into (19) yields

$$I_{150a} = \frac{5}{2} I_{50a}. \tag{20}$$

From (18) and (20), the rms value of i_{uv} and I_{uv}, is given by

$$I_{\mathrm{uv}} = \sqrt{I_{50a}^2 + I_{150a}^2} = \frac{\sqrt{29}}{5} I_{150a}. \tag{21}$$

Equation (21) and the relationship $I_{\mathrm{uv}} = I/\sqrt{3}$ produce the following equations:

$$I_{\mathrm{uv}} = \frac{I}{\sqrt{3}} = \frac{\sqrt{29}}{5} I_{150a}$$
$$I_{150a} = \frac{5}{\sqrt{87}} I. \tag{22}$$

The power rating of the transformer P_{Trans} is calculated from (9)–(11), and (22) as follows:

$$P_{\mathrm{Trans}} = 3aV_{\mathrm{S}} I_{150a} = 3 \times \frac{2}{5} V_{\mathrm{S}} \times I_{150a}$$
$$= \frac{6}{\sqrt{87}} V_{\mathrm{S}} I. \tag{23}$$

Hence, the ratio of P_{Trans} to the rated reactive power Q_{rated} $(= \sqrt{3} V_{\mathrm{S}} I)$ is

$$\frac{P_{\mathrm{Trans}}}{Q_{\mathrm{rated}}} = \frac{2}{\sqrt{29}} = 0.37. \tag{24}$$

In summary, the active power that can be exchanged via the transformer is limited to 37% of the rated reactive power.

D. Relationship Between Active and Reactive Power

No reactive power at the ac mains has been assumed in the previous section. Meanwhile, Fig. 2 circuit may control the active power and positive-sequence reactive power simultaneously in an actual situation. When the positive-sequence reactive power is controlled, a current that lags (or leads) the cluster voltage by 90° is superimposed on the cluster current. Let the 50-Hz current originating from the reactive power control be I_{50r}. Consequently, (18) becomes

$$i_{\mathrm{uv}} = \sqrt{2} I_{50a} \sin\left(\omega t + \frac{\pi}{6}\right) + \sqrt{2} I_{150a} \sin\left(3\omega t - \frac{\pi}{2}\right)$$
$$+ \sqrt{2} I_{50r} \sin\left(\omega t + \frac{\pi}{6} \pm \frac{\pi}{2}\right). \tag{25}$$

The third term on the right-hand side in (25) corresponds to the current originating from the reactive power control. It should be noted that this additional current has no effect on the analysis of the power rating of Fig. 2 circuit presented in the previous section, and (19) to (24) hold regardless of this additional current. The reason for this is that (19) always holds when the positive-sequence reactive power is controlled owing to the phase difference of 90° between the cluster voltage and the current. The cluster rms current should be less than or equal to $I/\sqrt{3}$ even when the active power and positive-sequence reactive power are controlled simultaneously.

Let the active and reactive power of the ac mains be P $(= 3V_{\mathrm{S}} I_{50a})$ and Q $(= 3V_{\mathrm{S}} I_{50r})$, and the rated reactive power be Q_{rated}, respectively. Fig. 4 shows the relationship between the active and reactive power under the rated cluster current of $I/\sqrt{3}$ (see Appendix). It should be noted that the vertical and horizontal axes are not proportional in Fig. 4. The active power of 37% of the rated reactive power can be exchanged when $Q = 0$, and the ratio decreases nonlinearly as Q increases. For example, the active power of 22% and the reactive power of 80% of the rated reactive power can be controlled simultaneously, according to Fig. 4. Finally, the relationship $P = 0$ holds when $Q = Q_{\mathrm{rated}}$. Furthermore, the converter losses of Figs. 1 and 2 are comparable as long as (10), (11), and Fig. 4 hold.

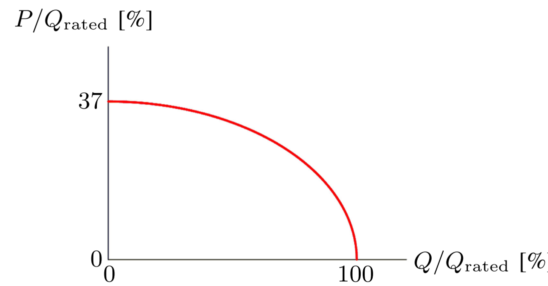

Fig. 4. Relationship between active power and reactive power under the rated cluster current of $I/\sqrt{3}$.

E. Ratings of L_{ac} and DC Capacitor Voltage

From (37) (see the Appendix), the u-phase supply current i_{u} is calculated as

$$i_{\mathrm{u}} = \sqrt{\frac{2}{3}} \frac{\sqrt{P^2 + Q^2}}{V_{\mathrm{S}}} \sin(\omega t + \alpha) \tag{26}$$

where α is given by (38). On the other hand, the following relationship holds from (40):

$$\sqrt{P^2 + Q^2} < Q_{\mathrm{rated}}. \tag{27}$$

The abovementioned equations imply that the supply rms current of Fig. 2 is less than the rated current of Fig. 1 working as a STATCOM for positive-sequence reactive power control, as long as Fig. 4 is satisfied. Furthermore, the switching-ripple current contained in i_{u} is the same between Figs. 1 and 2 because it is determined by the voltage step and switching frequency of each cell, and they are the same between them; hence, the same inductance can be applied. Hence, it is possible to apply L_{ac} used for Figs. 1 to 2 without any change.

Regarding the dc capacitor voltage of each cell, the dc voltage can be equal or less than that working as a STATCOM for positive-sequence reactive power control as long as ϕ and a are given by (10) and (11), respectively, because the cluster voltage can be equal or less than $\sqrt{2} V_{\mathrm{S}}$. Furthermore, the ac voltage contained in each dc capacitor voltage when the active and reactive power are controlled simultaneously is smaller in amplitude than that when the rated positive-sequence reactive power is controlled because of reasons that will be described in the last paragraph of Section V-C.

In summary, the same ratings of L_{ac}, dc voltage, and capacitance of each submodule can be applied to Figs. 1 and 2.

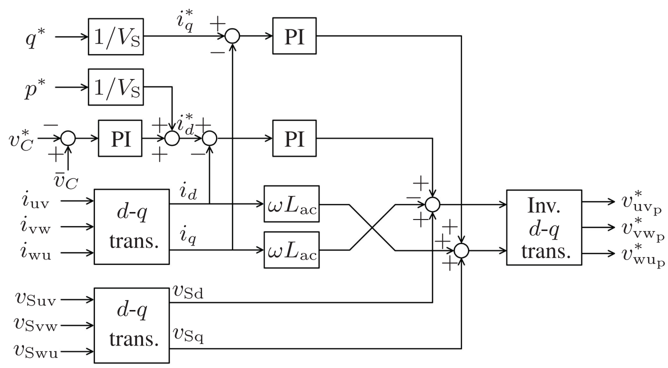

Fig. 5. Block diagram of instantaneous active and reactive power control, and overall voltage control.

IV. Control Method

The control method of the Fig. 2 circuit is divided into the following two parts:

1) control of the SDBC converter;
2) control of the single-phase converter.

A. Control of SDBC Converter

The control method of the SDBC converter can be classified into the following four subcontrols [9]:

1) active and reactive power control, and overall voltage control;
2) cluster-balancing control;
3) circulating-current control;
4) individual-balancing control.

Fig. 5 shows the control block diagram of the active and reactive power control, and the overall voltage control. p^* is the command value of the instantaneous active power, q^* is that of the instantaneous reactive power, i_d^* is that of the *d*-axis current, and i_q^* is that of the *q*-axis current. The overall voltage control is responsible for regulating $\bar{v}_C$, which is the arithmetic average voltage of all the floating dc capacitors used in the Fig. 2 circuit, to its command value v_C^*, and this is achieved by adjusting i_d^*. $\bar{v}_C$ is given by

$$\bar{v}_C = \frac{1}{3\,N} \sum_{o \in \{\mathrm{uv},\mathrm{vw},\mathrm{wu}\}} \sum_{i=1}^{N} \bar{v}_{Coi}. \tag{28}$$

A moving-average filter of 100 Hz is applied to each dc-capacitor voltage v_{Coi}, to detect only the dc component. The independent control of i_d and i_q is achieved by applying the conventional decoupled current control. Finally, Fig. 5 circuit produces the positive-sequence voltage commands of the three clusters $v_{\mathrm{uv_p}}^*$, $v_{\mathrm{vw_p}}^*$, and $v_{\mathrm{wu_p}}^*$.

When the active power is controlled, the command of the zero-sequence voltage v_{zero}^*, is added to the voltage commands, where it is given by

$$v_{\mathrm{zero}}^* = \sqrt{2} V_{\mathrm{zero}} \sin(3\omega t - \pi/2) \tag{29}$$

where V_{zero} is the rms value. Finally, the voltage commands of the three clusters v_{uv}^*, v_{vw}^*, and v_{wu}^* are given by

$$\begin{aligned} v_{\mathrm{uv}}^* &= v_{\mathrm{uv_p}}^* - v_{\mathrm{zero}}^* \\ v_{\mathrm{vw}}^* &= v_{\mathrm{vw_p}}^* - v_{\mathrm{zero}}^* \\ v_{\mathrm{wu}}^* &= v_{\mathrm{wu_p}}^* - v_{\mathrm{zero}}^*. \end{aligned} \tag{30}$$

It should be noted that v_{zero}^* corresponds to $v_{\mathrm{T2\_150}}$ described in Section III-B, and the relationship $v_{\mathrm{T2\_150}} = 3v_{\mathrm{zero}}^*$ holds.

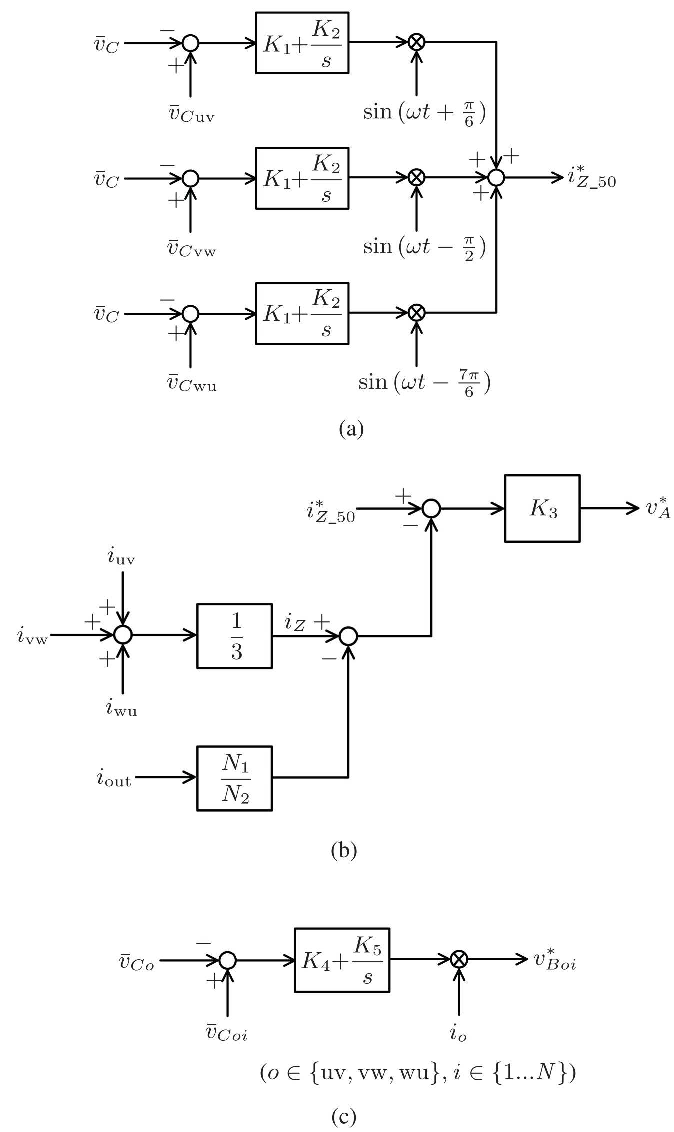

Fig. 6. Block diagram of dc-capacitor voltage control. (a) Cluster-balancing control. (b) Circulating-current control. (c) Individual-balancing control.

1) Cluster-Balancing Control: Fig. 6(a) shows the control block diagram of the cluster-balancing control. It is responsible for balancing the arithmetic average voltage of each phase, $\bar{v}_{Co}$, to $\bar{v}_C$ by adjusting the 50-Hz component included in i_Z, i_{Z_50}. $\bar{v}_{Co}$ is given by

$$\bar{v}_{Co} = \frac{1}{N} \sum_{i=1}^{N} \bar{v}_{Coi}. \tag{31}$$

It is noteworthy that $\sin(\omega t + \frac{\pi}{6})$ in Fig. 6(a) is in phase with the 50-Hz positive-sequence component included in v_{uv}.

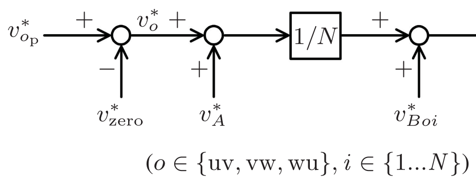

Fig. 7. Voltage command of each bridge cell.

When $\bar{v}_{C\mathrm{uv}} > \bar{v}_C$, the product of v_uv and i_{Z_50} forms the positive active power because the command of i_{Z_50}, $i^*_{Z\_50}$, contains the same frequency component that is in phase with v_uv. Consequently, the cluster discharges positive active power, decreasing $\bar{v}_{C\mathrm{uv}}$. Meanwhile, the product of v_uv and i_{Z_50} forms negative active power when $\bar{v}_{C\mathrm{uv}} < \bar{v}_C$, increasing $\bar{v}_{C\mathrm{uv}}$.

2) Circulating-Current Control: Fig. 6(b) shows the control block diagram of the circulating-current control. The circulating current i_Z given by (4) contains the 150-Hz component in addition to the 50-Hz component. The control is achieved by utilizing the 50-Hz component included in i_Z, as described in [9], so that the 150-Hz component is eliminated from the control system. There are two methods to eliminate the 150-Hz component as follows:

1) using a moving-average filter of 150 Hz;
2) using the primary current of the transformer.

This article uses the latter method because the 150-Hz component can be detected without any control delay. To be specific, the 150-Hz component is eliminated from i_Z using the detected primary current and the turns ratio of the transformer, as shown in Fig. 6(b). Finally, the command voltage v^*_A, which is common to each phase, is generated. It should be noted that v^*_A corresponds to v_{T2_50} described in Section III-B, and the relationship $v_{\mathrm{T2}\_50} = 3v^*_A$ holds.

3) Individual-Balancing Control: Fig. 6(c) shows the control block diagram of the individual-balancing control. It forces each dc-capacitor voltage $\bar{v}_{Coi}$ to follow $\bar{v}_{Co}$. The voltage command v^*_{Boi} is given by

$$v^*_\mathrm{Boi} = \left(K_4(\bar{v}_{Coi} - \bar{v}_{Co}) + K_5 \int (\bar{v}_{Coi} - \bar{v}_{Co})dt\right) i_o. \quad (32)$$

It forms active power between v^*_Boi and i_o, thereby achieving voltage balancing. Equation (32) implies that the sum of the voltage commands in one cluster is equal to zero. This means that no interference occurs between the individual-balancing control and the current control.

Fig. 7 shows the control block diagram of the voltage command of each bridge cell. The ac voltage command v^*_{oi} is given by

$$v^*_{oi} = \frac{v^*_{o_\mathrm{p}} - v^*_\mathrm{zero} + v^*_A}{N} + v^*_\mathrm{Boi} = \frac{v^*_o + v^*_A}{N} + v^*_\mathrm{Boi}. \quad (33)$$

B. Difference in Control Between Figs. 1 and 2 Circuits

The control method of the Fig. 2 circuit is basically the same as that of the Fig. 1 circuit except for the following differences.

1) The primary current i_out is taken into the circulating-current control shown in Fig. 6(b).

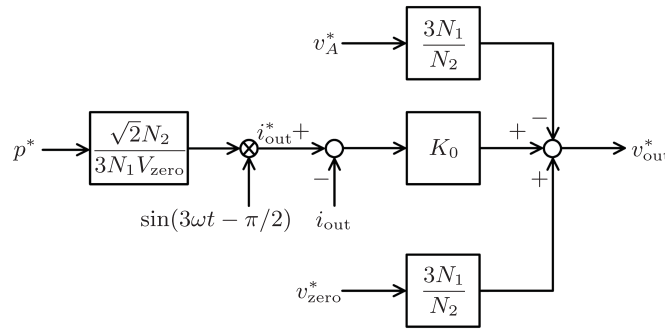

Fig. 8. Block diagram of current control of the single-phase medium-frequency converter.

2) The voltage command for the zero-sequence voltage v^*_zero, is added to v^*_{oi}, as shown in Fig. 7.
3) The values of p^*, v^*_zero, and v^*_A are given to the control system of the single-phase inverter, as will be shown in Fig. 8.

C. Control of Single-Phase Converter

Fig. 8 shows the control block diagram of the single-phase medium-frequency converter. The current command of i_out, i^*_out, is given by

$$i^*_\mathrm{out} = \frac{\sqrt{2}p^* N_2}{3N_1 V_\mathrm{zero}} \sin(3\omega t - \pi/2). \quad (34)$$

Equations (9), (10), and (34) indicate that v_T2 and i^*_out are in phase. The conventional proportional control with the control gain K_0 is applied to the current feedback control. Finally, the ac voltage command v^*_out is given by

$$v^*_\mathrm{out} = K_0(i^*_\mathrm{out} - i_\mathrm{out}) + \frac{3N_1}{N_2}v^*_\mathrm{zero} - \frac{3N_1}{N_2}v^*_A. \quad (35)$$

The second term on the right-hand side in (35) corresponds to the medium-frequency voltage applied to the transformer by the SDBC converter. Meanwhile, the third term plays an important role in eliminating the 50-Hz component from the primary circuit.

D. Relationship Between Current Controllability and Inductance

Fig. 2 circuit controls the supply currents (i_u, i_v, and i_w), the 50-Hz fundamental-frequency component included in i_Z, i_{Z_50}, and the primary current of the transformer i_out, and each control is independent. Meanwhile, the inductance that affects the current controllability is different in each current. To be specific, the controllability of the supply currents is determined by the ac-link inductor L_ac, that of i_{Z_50} is determined by the magnetizing inductance L_M represented by (14), and that of i_out is determined by the ac inductor L_con including the leakage inductance of the transformer.

In general, L_M is greater than L_ac or L_con, as can be observed in Table I. This implies that each cell should produce a larger voltage to achieve fast current controllability of i_{Z_50}.

TABLE I
SPECIFICATIONS OF THE EXPERIMENTAL MODEL

Nominal line-to-line voltage	V_{S}	110 V
Line frequency	$\omega/2\pi$	50 Hz
Transformer frequency	$\omega_{\mathrm{Trans}}/2\pi$	150 Hz
Rated reactive power	Q_{rated}	5 kVA
Rated supply current	I	26.2 A
Rated cluster current	$I/\sqrt{3}$	15.2 A
Rated active power	P_{rated}	1.85 kW
Bridge-cell count	N	6
AC-link inductor	L_{ac}	0.3 mH
Magnetizing inductance	L_M	82 mH
DC capacitor	C	47 mF
DC-capacitor voltage	V_C	28 V
Zero-sequence voltage	V_{zero}	40 V
Carrier frequency of each cell	$\omega_{\mathrm{c,cell}}/2\pi$	1 kHz
Equivalent switching frequency	$\omega_{\mathrm{sw,eq}}/2\pi$	12 kHz
Transformer primary voltage	V_{T1}	120 V
Transformer secondary voltage	V_{T2}	120 V
Transformer primary current	I_{out}	15.4 A
Turns ratio	N_2/N_1	1
DC voltage	V_{dc}	200 V
AC inductor	L_{con}	0.18 mH
Carrier frequency of converter	$\omega_{\mathrm{c,con}}/2\pi$	6 kHz

When the active power or positive-sequence reactive power is controlled, the relationship $i_{Z\_50} = 0$ always holds because the power imbalance between clusters does not occur inherently in both steady- and transient-state conditions. However, the fast current controllability of i_{Z_50} may be required when the negative-sequence reactive power is controlled where the power imbalance between clusters is inherent and the relationship $i_{Z\_50} = 0$ does not hold [9]; such a situation can occur under grid fault conditions. In order to achieve fast current controllability of i_{Z_50}, L_M needs to be reduced, which can be achieved by introducing appropriately designed air gap(s) to the transformer.

V. EXPERIMENT

A. Experimental Conditions

Fig. 9 shows a photograph of a downscaled 110-V, 5-kVA model that is used to verify the circuit of Fig. 2. The SDBC converter used in experiments is the same as the one used in [20] and [21], except for some modifications in the circuit parameters. Table I summarizes the circuit parameters used in the experiments. The rated active power is $P_{\mathrm{rated}} = 1.85$ kW, which corresponds to 37% of the rated reactive power $Q_{\mathrm{rated}} = 5$ kVA, according to Fig. 4. The rated supply and cluster rms currents are $I = 26.2$ A and $I/\sqrt{3} = 15.2$ A, respectively. The zero-sequence voltage is set to $V_{\mathrm{zero}} = 40$ V, which is approximately 40% of the supply line-to-line voltage, according to (17).

The supply line-to-neutral voltages v_{Su}, v_{Sv}, and v_{Sw} are calculated as follows:

$$v_{\mathrm{Su}} = \frac{v_{\mathrm{Suv}} - v_{\mathrm{Swu}}}{3}$$
$$v_{\mathrm{Sv}} = \frac{v_{\mathrm{Svw}} - v_{\mathrm{Suv}}}{3}$$
$$v_{\mathrm{Sw}} = \frac{v_{\mathrm{Swu}} - v_{\mathrm{Svw}}}{3}.$$

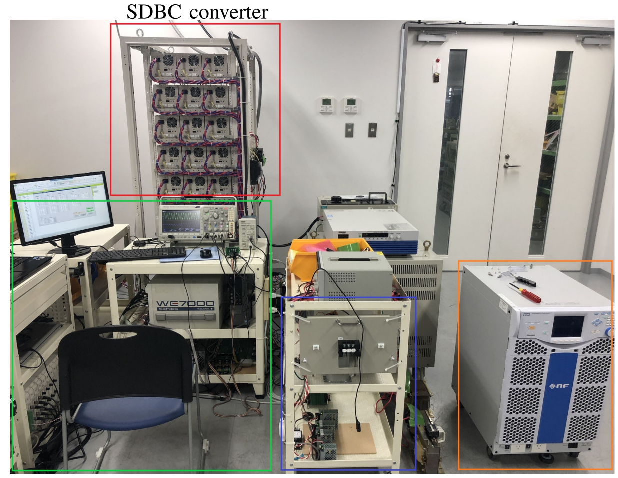

Fig. 9. Photograph of the downscaled 110-V, 5-kVA model.

The bridge-cell count used in each cluster is $N = 6$, and the carrier frequency of each cell is 1 kHz. The phase-shifted PWM with a phase difference of 30° (= 180°/N) is applied to each cell, so that the equivalent switching frequency of the cluster is 12 kHz (= $2 \times 6 \times 1$ kHz). The turns ratio of the transformer is set to $N_2/N_1 = 1$. The single-phase converter is implemented using the traditional single-phase full-bridge PWM converter with a carrier frequency of 6 kHz. The dc voltage V_{dc} is implemented using the NF Corporation DP030RS, which is capable of regenerative operation, and it is set to 200 V.

The control system consists of a digital signal processor unit that uses the Texas Instruments TMS320C6713 and a field-programmable gate array (FPGA) unit using the Altera Cyclone II. The FPGA unit, which includes A/D converters, detects the 18 dc-capacitor voltages of each chopper cell, the three cluster currents, the two supply voltages, the dc source voltage, and the transformer primary current. The FPGA unit produces 76-bit gate signals. The experimental waveforms except for i_{out} and v_{T1} were captured using the Yokogawa WE7000. The waveform of i_{out} was captured using the Tektronix TCP303 with a frequency band of 15 MHz, and that of v_{T1} was captured using the Tektronix P5205 with a frequency band of 100 MHz.

B. Steady-State Operation When Active Power is Controlled

Fig. 10 shows the experimental waveforms under steady state when $p^* = 1.85$ kW (37%) and $q^* = 0$, where Fig. 10(a) shows the SDBC-side waveforms and Fig. 10(b) shows the converter-side waveforms. The voltage and current waveforms correspond to those shown in Fig. 2. Because the relationships $p^* > 0$ and $q^* = 0$ hold, positive active power flows from the dc source to the three-phase ac mains with unity power factor.

The cluster voltages v_{uv}, v_{vw}, and v_{wu} are 12-level multilevel waveforms with fewer harmonic voltages owing to the favorable effect of the phase-shifted PWM, where v_{uv} is given by (17). Hence, the amplitude of the 150-Hz component is 40% that of the 50-Hz component. The supply currents i_{u}, i_{v}, and i_{w} are the three-phase balanced current, and they are in phase with the

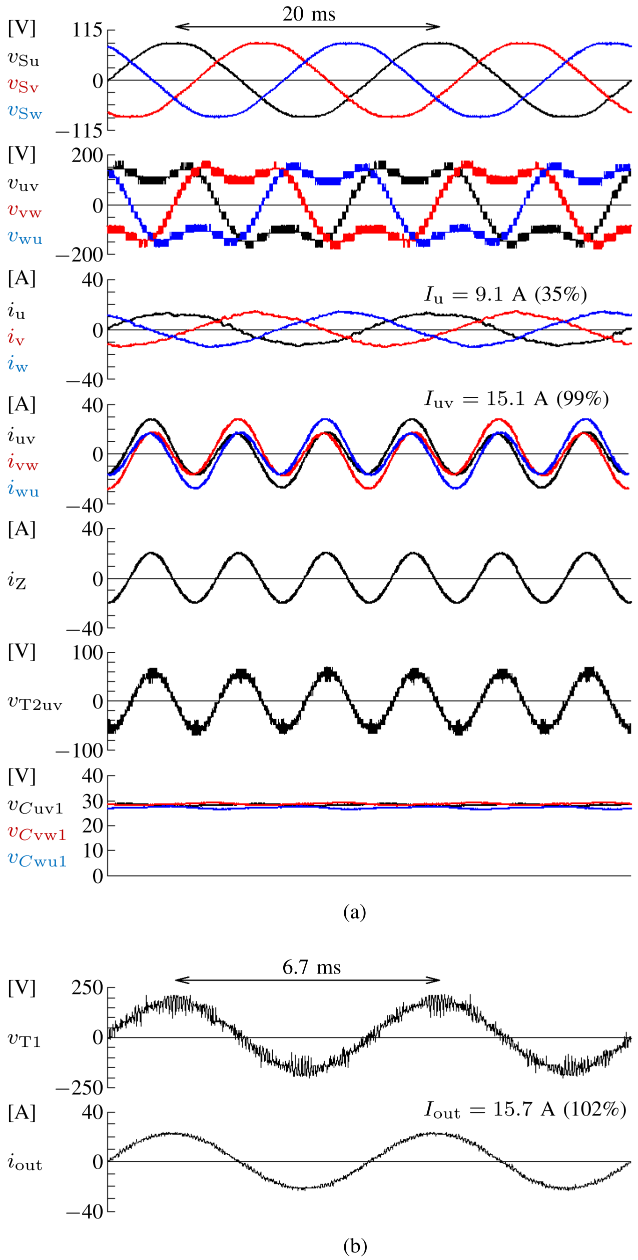

Fig. 10. Experimental steady-state waveforms when $p^* = 1.85$ kW (37%) and $q^* = 0$. (a) SDBC-side waveforms. (b) Converter-side waveforms.

supply voltages v_{Su}, v_{Sv}, and v_{Sw}, respectively. The rms value of i_{u}, I_{u}, is 9.1 A, which corresponds to 35% of the rated current of 26.2 A. It is smaller than the theoretical current of 9.7 A (37%) because the losses in the SDBC converter and transformer are fed by the three-phase ac mains.

The cluster currents i_{uv}, i_{vw}, and i_{wu} contain two frequency components: the 50-Hz line-frequency component and the 150-Hz component. From (20), the amplitude of the 50-Hz component is 40% that of the 150-Hz component. The rms value of i_{uv}, I_{uv}, is 15.1 A, which corresponds to 99% of the rated cluster current of 15.2 A. The circulating current i_{Z} comprises the dominant 150-Hz component (i.e., i_{Za_150}), where (16) holds, considering that i_{Z_50} given by (13) and i_{Zm_150} given by (15) are small enough to be negligible. Finally, the relationship $i_{\mathrm{Z}} = i_{\mathrm{out}}$ holds based on Table I.

The transformer secondary voltage v_{T2uv} is given by (9), where the relation $a = 2/5$ holds. Hence, the rms value of v_{T2uv}, V_{T2uv}, is theoretically 40 V, which agrees well with the experimental result of 41.6 V. The dc-capacitor voltages $v_{C\mathrm{uv1}}$, $v_{C\mathrm{vw1}}$, and $v_{C\mathrm{wu1}}$ contain the dc and ac components, and the dc component is regulated to 28 V. The peak-to-peak ac component is 1.2 V (4.3%).

The transformer primary voltage v_{T1} is given by $v_{\mathrm{T1}} = (N_1/N_2)v_{\mathrm{T2}}$, according to Fig. 3, and the relationship $v_{\mathrm{T2}} = 3v_{\mathrm{T2uv}}$ holds from (8). Hence, the rms value of v_{T1} is 120 V theoretically, which agrees well with the experimental result of 122 V. The transformer primary current i_{out} is controlled to be in phase with the fundamental component included in the ac voltage of the single-phase converter, v_{out}. The rms value of i_{out}, I_{out}, is 15.7 A, which corresponds to 102% of the rated current of 15.4 A. Consequently, the actual active power fed by the dc source is 1.88 kW ($= 120\,\mathrm{V} \times 15.7\,\mathrm{A}$), which corresponds to 102% of the rated power of 1.85 kW.

Fig. 11 shows the experimental waveforms under steady state when $p^* = -1.85$ kW (-37%) and $q^* = 0$, where Fig. 11(a) shows the SDBC-side waveforms and Fig. 11(b) shows the converter-side waveforms. Because the relationships $p^* < 0$ and $q^* = 0$ hold, positive active power flows from the three-phase ac mains to the dc source with unity power factor. The supply currents i_{u}, i_{v}, and i_{w} are out of phase with the supply voltages v_{Su}, v_{Sv}, and v_{Sw} by 180°, respectively. Furthermore, the 150-Hz components included in the three cluster currents i_Z, and i_{out} are out of phase with those shown in Fig. 10 because of the power-flow inversion. The other waveforms are similar to those shown in Fig. 10.

C. Steady-State Operation When Active and Reactive Power are Controlled Simultaneously

Fig. 12 shows the experimental waveforms under steady state when $p^* = 1.1$ kW (22%) and $q^* = 4.0$ kVA (80%), where Fig. 12(a) shows the SDBC-side waveforms and Fig. 12(b) shows the converter-side waveforms. Because $p^* > 0$ and $q^* > 0$, positive active power flows from the dc source to the three-phase ac mains, and the SDBC converter provides leading reactive power to the supply. The rms value of the supply current i_{u}, I_{u}, is increased to 21.8 A, which corresponds to 83% of the rated current of 26.2 A. However, the rms value of the cluster current i_{uv}, I_{uv}, is 15.2 A, which is the same as the rated current of 15.2 A because p^* and q^* are given according to Fig. 4. Meanwhile, the amplitudes of the 150-Hz components included in the three cluster currents i_Z, and i_{out} are smaller than those shown in Figs. 10 and 11 because of the reduced active power. The peak-to-peak ac component included in the dc-capacitor voltages $v_{C\mathrm{uv1}}$, $v_{C\mathrm{vw1}}$, and $v_{C\mathrm{wu1}}$ is 1.2 V (4.3%), which is the same as the one shown in Figs. 10 and 11.

It is noteworthy that the ac component included in the dc-capacitor voltages $v_{C\mathrm{uv1}}$, $v_{C\mathrm{vw1}}$, and $v_{C\mathrm{wu1}}$ when $p^* = 0$ and

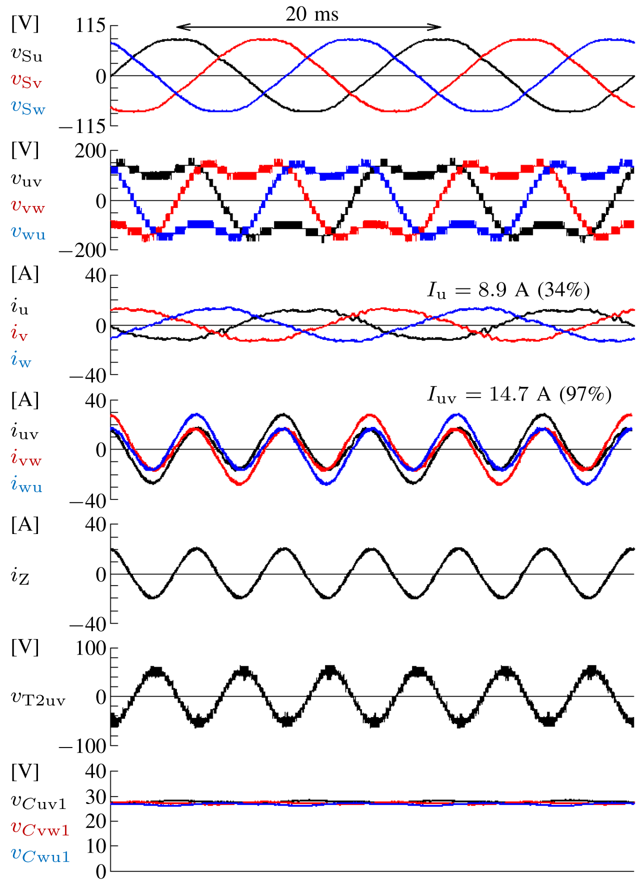

(a)

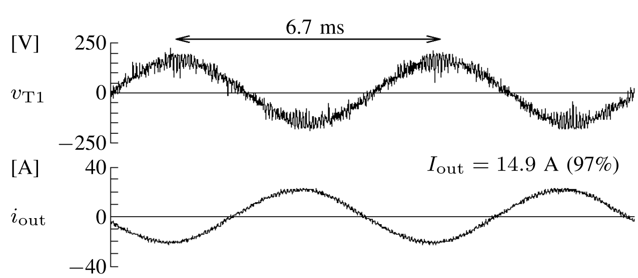

(b)

Fig. 11. Experimental steady-state waveforms when $p^* = -1.85$ kW (-37%) and $q^* = 0$. (a) SDBC-side waveforms. (b) Converter-side waveforms.

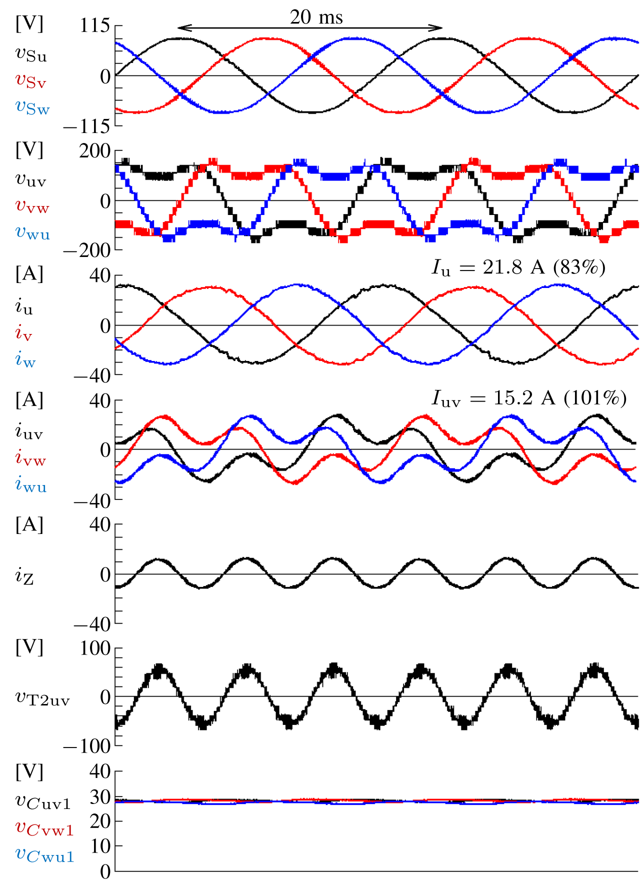

(a)

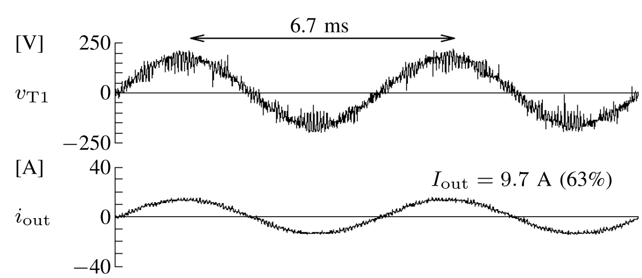

(b)

Fig. 12. Experimental steady-state waveforms when $p^* = 1.1$ kW (22%) and $q^* = 4.0$ kVA (80%). (a) SDBC-side waveforms. (b) Converter-side waveforms.

$q^* = 5.0$ kVA (100%) was obtained experimentally as 1.5 V (5.3%). This indicates that the ac component when the active and reactive power are controlled simultaneously is smaller than that when the rated reactive power is controlled as long as the relationship shown in Fig. 4 is satisfied. The reason for this is that the ac component is inversely proportional to the frequency [9], and the ac voltage fluctuation originating from the 150-Hz component is smaller than that originating from the 50-Hz component. The other waveforms are similar to those shown in Figs. 10 and 11.

D. Transient-State Operation When Active Power is Controlled

Fig. 13 shows the experimental transient waveforms when p^* was changed from zero to 1.85 kW under a ramp change in 50 ms while q^* was kept zero. It was confirmed that each current follows the command with good accuracy with no overcurrent. It is evident from the dc-capacitor voltages that their dc components are well regulated to the command value of 28 V even in transient-state conditions. The Fig. 2 circuit can achieve fast power-flow control because the current controllability of the supply current is determined by the ac-link inductor L_{ac} and that of the transformer primary current is determined by

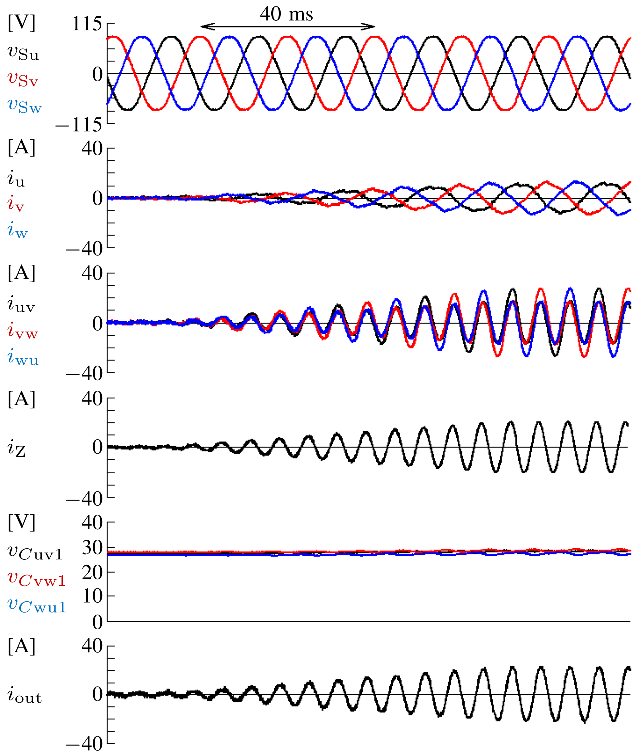

Fig. 13. Experimental transient waveforms when p^* was changed from zero to 1.85 kW under a ramp change in 50 ms while q^* was kept zero.

the ac inductor $L_{\rm con}$, both of which are much smaller than the magnetizing inductance L_M, as shown in Table I.

VI. Conclusion

This article has described a dc/1ϕ/3ϕ power converter that combines the SDBC converter with a medium-frequency single-phase converter via a single-phase transformer with an operating frequency of 150 Hz. Its characteristic is that the active power of 37% of the rated reactive power can be controlled between the dc source and the three-phase ac mains without increasing the voltage and current ratings of the SDBC converter, thereby achieving transient stability improvement and superior voltage regulation of electric power systems. The operating principles and control method have been verified by experiments using a downscaled 110-V, 5-kVA model.

Appendix

Relationship Between Active and Reactive Power

The cluster current $i_{\rm uv}$ given by (25) can be changed with the help of the relationships $P = 3V_{\rm S}I_{50a}$, $Q = 3V_{\rm S}I_{50r}$, and (20) as follows:

$$i_{\rm uv} = \frac{\sqrt{2}P}{3V_{\rm S}}\sin\left(\omega t + \frac{\pi}{6}\right) + \frac{5}{2}\frac{\sqrt{2}P}{3V_{\rm S}}\sin\left(3\omega t - \frac{\pi}{2}\right) + \frac{\sqrt{2}Q}{3V_{\rm S}}\sin\left(\omega t + \frac{\pi}{6} \pm \frac{\pi}{2}\right). \tag{36}$$

Based on the compositions of trigonometric functions, (36) can be changed to

$$i_{\rm uv} = \frac{\sqrt{2}}{3V_{\rm S}}\left(\sqrt{P^2+Q^2}\sin\left(\omega t + \frac{\pi}{6} + \alpha\right) + \frac{5}{2}P\sin\left(3\omega t + \frac{\pi}{2}\right)\right) \tag{37}$$

where α is given by

$$\alpha = \pm\tan^{-1}\frac{Q}{P}. \tag{38}$$

In (37), the rated cluster rms current should be the same as the one obtained when $P = 0$ and $Q = Q_{\rm rated}$. Hence, the following relationship holds:

$$\left(\frac{Q_{\rm rated}}{3V_{\rm S}}\right)^2 = \left(\frac{1}{3V_{\rm S}}\right)^2\left(P^2 + Q^2 + \left(\frac{5}{2}P\right)^2\right). \tag{39}$$

Finally, the following relationship holds among P, Q, and $Q_{\rm rated}$

$$P = \frac{2}{\sqrt{29}}\sqrt{Q_{\rm rated}^2 - Q^2} = 0.37\sqrt{Q_{\rm rated}^2 - Q^2}. \tag{40}$$

References

[1] T. Fujii *et al.*, “A MVA GCT STATCOM for the Kanzaki substation,” in *Proc. IEEJ Int. Power Electron.*, 2005, pp. 1299–1306.
[2] T. Fujii *et al.*, “Coordinated voltage control and continuous operation of the 80 MVA STATCOM under commercial operation,” in *Proc. IEEJ Power Convers. Conf.*, pp. 969–974, 2007.
[3] T. Fujii, K. Temma, N. Morishima, T. Akedani, T. Shimonosono, and H. Harada, “450 MVA GCT-STATCOM for stability improvement and over-voltage suppression,” in *Proc. IEEJ Int. Power Electron.*, 2010, pp. 1776–1782.
[4] J. S. Lai and F. Z. Peng, “Multilevel converters-a new breed of power converters,” *IEEE Trans. Ind. Appli.*, vol. 32, no. 3, pp. 509–517, May/Jun. 1996.
[5] F. Z. Peng and J. Wang, “A universal STATCOM with delta-connected cascade multilevel inverter,” in *Proc. IEEE Power Electron. Specialists Conf.*, 2004, pp. 3529–3533.
[6] H. Akagi, “Classification, terminology, and application of the modular multilevel cascade converter (MMCC),” *IEEE Trans. Power Electron.*, vol. 26, no. 11, pp. 3119–3130, Nov. 2011.
[7] K. Fujii, U. Schwarzer, and R. W. De Doncker, “Comparison of hard-switched multi-level inverter topologies for STATCOM by loss-implemented simulation and cost estimation,” in *Proc. IEEE Power Electron. Specialists Conf.*, 2005, pp. 340–346.
[8] K. Fujii, R. W. De Doncker, and S. Konishi, “A novel dc-link voltage control of PWM-switched cascade cell multi-level inverter applied to STATCOM,” in *Proc. IEEE Industry Appl. Soc.*, 2005, pp. 961–967.
[9] M. Hagiwara, R. Maeda, and H. Akagi: “Negative-sequence reactive-power control by a PWM STATCOM based on a modular multilevel cascade converter (MMCC-SDBC),” *IEEE Trans. Ind. Appl.*, vol. 48, no. 2, pp. 720–729, Mar./Apr. 2012.
[10] S. Du, J. Liu, J. Lin, and Y. He, “A novel DC voltage control method for STATCOM based on hybrid multilevel h-bridge converter,” *IEEE Trans. Power Electron.*, vol. 28, no. 1, pp. 101–111, Jan. 2013.
[11] Y. Koyama, T. Arai, R. Hasegawa, and D. Suzuki, “One-pulse control for modular multilevel converter based STATCOM,” in *Proc. 18th Eur. Conf. Power Electron. Appl.*, 2016, pp. 1–10.
[12] E. Behrouzian and M. Bongiorno, “Investigation of negative-sequence injection capability of cascaded h-bridge converters in star and delta configuration,” *IEEE Trans. Power Electron.*, vol. 32, no. 2, pp. 1675–1683, Feb. 2017.

[13] P. -H. Wu, H. -C. Chen, Y. -T. Chang, and P. -T. Cheng, "Delta-connected cascaded h-bridge converter application in unbalanced load compensation," *IEEE Trans. Ind. Appli.*, vol. 53, no. 2, pp. 1254–1262, Mar./Apr. 2017.
[14] Z. He *et al.*, "Reactive power strategy of cascade delta-connected STATCOM under asymmetrical voltage conditions," *IEEE Trans. Emerg. Sel. Topics Power Electron.*, vol. 5, no. 2, pp. 784–795, Jun. 2017.
[15] D. Sullivan *et al.*, "Application of FACTS devices for a dynamic power system within the USA," in *Proc. Int. Power Electron. Conf.-Niigata*, 2018, pp. 2329–2334.
[16] J.-J. Jung, J. -H. Lee, S.-K. Sul, G. T. Son, and Y.-H. Chung, "DC capacitor voltage balancing control for delta-connected cascaded h-bridge STATCOM considering unbalanced grid and load conditions," *IEEE Trans. Power Electron.*, vol. 33, no. 3, pp. 4726–4735, Jun. 2018.
[17] P. -H. Wu and P. -T. Cheng, "A fault-tolerant control strategy for the delta-connected cascaded converter," *IEEE Trans. Power Electron.*, vol. 33, no. 12, pp. 10946–10953, Dec. 2018.
[18] V. Spudić and T. Geyer, "Model predictive control based on optimized pulse patterns for modular multilevel converter STATCOM," *IEEE Trans. Ind. Appl.*, vol. 55, no. 6, pp. 6137–6149, Nov./Dec. 2019.
[19] L. Maharjan, T. Tajyuta, K. Maruyama, A. Suzuki, and A. Toba, "Development and verification test of the 6.6-kV 200-kVA transformerless SDBC-based STATCOM using SiC-MOSFET modules," *IEEE Trans. Power Electron.*, vol. 35, no. 12, pp. 13687–13696, Dec. 2020.
[20] P. Sochor and H. Akagi, "Theoretical comparison in energy-balancing capability between star- and delta-congured modular multilevel cascade inverters for utility-scale photo-voltaic systems," *IEEE Trans. Power Electron.*, vol. 31, no. 3, pp. 1980–1992, Mar. 2016.
[21] P. Sochor and H. Akagi, "Theoretical and experimental comparison between phase-shifted PWM and level-shifted PWM in a modular multilevel SDBC inverter for utility-scale photovoltaic applications," *IEEE Trans. Ind. Appl.*, vol. 53, no. 5, pp. 4695–4707, Sep./Oct. 2017.
[22] M. Hagiwara and H. Akagi, "High-voltage high-power conversion systems based on cutting-edge power devices and medium-frequency transformers," in Proc. *IEEJ Industry Appl. Soc.*, 2014, pp. 73–78, (*in Japanese*).
[23] Power converter, by H. Akagi and M. Hagiwara. (Oct. 16, 2018). US 10,103, 645 B2.
[24] Power converter, by H. Akagi and M. Hagiwara. (Aug. 22, 2018). *EP* 3 121 949 B1.
[25] M. Glinka and R. Marquardt, "A new ac/ac multilevel converter family," *IEEE Trans. Ind. Electron.*, vol. 52, no. 3, pp. 662–669, Jun. 2005.
[26] M. A. Perez, J. Rodriguez, E. J. Fuentes, and F. Kammerer, "Predictive control of AC-AC modular multilevel converters," *IEEE Trans. Ind. Electron.*, vol. 59, no. 7, pp. 2832–2839, Jul. 2012.
[27] N. Thitichaiworakorn, M. Hagiwara, and H. Akagi, "A medium-voltage large wind turbine generation system using an AC/AC modular multilevel cascade converter," *IEEE Trans. Emerg. Sel. Topics Power Electron.*, vol. 4, no. 2, pp. 534–546, Jun. 2016.
[28] S. Song, J. Liu, S. Ouyang, X. Chen, and B. Liu, "Control of direct AC/AC modular multilevel converter in railway power supply system," in *Proc. Int. Power Electron. Conf.-Niigata*, 2018, pp. 1051–1055.
[29] K. Suzuki and T. Takeshita, "Quick charger for a battery using modular matrix converter (MMxC)," in *Proc. Int. Power Electron. Conf.-Niigata*, 2018, pp. 3501–3506.
[30] Z. He, P. Guo, Z. Shuai, Q. Xu, A. Luo, and J. M. Guerrero, "Modulated model predictive control for modular multilevel AC/AC converter," *IEEE Trans. Power Electron.*, vol. 34, no. 10, pp. 10359–10372, Oct. 2019.
[31] L. Bessegato, K. Ilves, L. Harnefors, S. Norrga, and S. Qstlund, "Control and admittance modeling of an AC/AC modular multilevel converter for railway supplies," *IEEE Trans. Power Electron.*, vol. 35, no. 3, pp. 2411–2423, Mar. 2020.
[32] D. Sha, Z. Guo, and X. Liao "Cross-feedback output-current-sharing control for input-series-output-parallel modular DC-DC converters," *IEEE Trans. Power Electron.*, vol. 25, no. 11, pp. 2762–2771, Nov. 2010.

Makoto Hagiwara (Senior Member, IEEE) was born in Tokyo, Japan, in 1979. He received the B.S., M.S., and Ph.D. degrees in electrical engineering from the Tokyo Institute of Technology, Tokyo, Japan, in 2001, 2003, and 2006, respectively.

From April 2006 to March 2015, he was an Assistant Professor with the Department of Electrical and Electronic Engineering, Tokyo Institute of Technology. Since April 2015, he has been an Associate Professor in the same institute. His research interests include dc-to-dc converters for electric trains/vehicles, high-voltage high-power converters for utility applications and renewable energies, and HVdc technologies.

Dr. Hagiwara received the 2010 International Power Electronics Conference (IPEC-Sapporo/ECCE-Asia) Second Prize Paper Award, the 2012 and 2013 IEEE Industry Applications Society Industrial Power Converter Committee First Prize Paper Awards, and the 2014 Isao Takahashi Power Electronics Award. The total citation index for all his papers in Google Scholar is more than 5,600.

Yoshihito Chuman was born in Miyazaki, Japan, in 1994. He received the B.S. degree in electrical engineering, and the M.S. degree in electrical and electronic engineering from the Tokyo Institute of Technology, Tokyo, Japan, in 2019 and 2021, respectively.

Since April 2021, he has been with Chukyo TV. Broadcasting Co., Ltd.

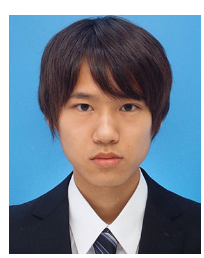

Yuki Kudo was born in Aomori, Japan, in 1994. He received the B.S. degree in electrical engineering and the M.S. degree in electrical and electronic engineering from the Tokyo Institute of Technology, Tokyo, Japan, in 2017 and 2019, respectively.

Since April 2019, he has been with Toshiba Energy Systems and Solutions Corporation.